Liquid Crystals
Publication details, including instructions for authors and subscription information:
http://www.informaworld.com/smpp/title~content=t713926090

Mesomorphic behaviour, single crystal and low angle variable temperature X-ray diffraction studies of the chloro-bridged cyclopalladated dimer obtained from 4,4'-hexyloxyazobenzene

A. Crispini[a]; M. Ghedini[a]; S. Morrone[a]; D. Pucci[a]; O. Francescangeli[b]
[a] Dipartimento di Chimica, Universita' della Calabria, Arcavacata, CS, Italy [b] Dipartimento di Scienze dei Materiali e della Terra, Sezione Fisica, Università di Ancona, Ancona, Italy

To cite this Article Crispini, A. , Ghedini, M. , Morrone, S. , Pucci, D. and Francescangeli, O.(1996) 'Mesomorphic behaviour, single crystal and low angle variable temperature X-ray diffraction studies of the chloro-bridged cyclopalladated dimer obtained from 4,4'-hexyloxyazobenzene', Liquid Crystals, 20: 1, 67 — 76
To link to this Article: DOI: 10.1080/02678299608032028
URL: http://dx.doi.org/10.1080/02678299608032028

LIQUID CRYSTALS, 1996, VOL. 20, NO. 1, 67–76

Mesomorphic behaviour, single crystal and low angle variable temperature X-ray diffraction studies of the chloro-bridged cyclopalladated dimer obtained from 4,4′-hexyloxyazobenzene

by A. CRISPINI, M. GHEDINI,* S. MORRONE, D. PUCCI
Dipartimento di Chimica, Universita' della Calabria, I-87030 Arcavacata (CS), Italy

and O. FRANCESCANGELI
Dipartimento di Scienze dei Materiali e della Terra, Sezione Fisica, Università di Ancona, Via Brecce Bianche, I-60131 Ancona, Italy

(*Received 21 April 1995; in final form 10 July 1995; accepted 27 July 1995*)

The newly synthesized palladium complex $[(\mathbf{Azo\text{-}6})Pd(\mu\text{-}Cl)]_2$, **1**, [**H(Azo-6)** = 4,4′-hexyloxyazobenzene] has been investigated by optical observations, calorimetric measurements, and single crystal and low angle variable temperature X-ray diffraction techniques. Two different mesophases appear from 210 to 220°C (nematic) and above 220 until 235°C (smectic E) where the compound eventually decomposes. The nematic phase is not in thermodynamic equilibrium and when subjected to an annealing process transforms into a smectic phase. The molecular structure of the dinuclear cyclopalladated complex **1** has an intramolecular Pd–Pd distance of 3·528(1) Å. Moreover the molecules of **1** are arranged in pairs with an intermolecular Pd–Pd non-bonded interaction distance of 3·668(1) Å. On the basis of this structural feature and of the variable temperature low-angle XRD studies, transitions involving dissociation of the molecular pairs (e.g. $N(pair) \rightleftharpoons S_E(single)$, on heating; $N(pair) \rightarrow S_E(pair)$, at constant temperature) are suggested.

1. Introduction

The thermotropic liquid crystalline properties of orthopalladated azo [1, 2] and arylimine [3, 4] systems are of considerable interest in the context of new mesomorphic materials [5].

Since the mesomorphic behaviour of dinuclear cyclopalladated complexes was found to be correlated with (i) the type of bridging ligand and (ii) the type of substituent in the organic part of the molecule, the examination of their crystal structures is becoming critical to the comprehension of these systems [6–8]. Comparisons between structural characteristics of the crystalline phase and the mesophase(s) of metallomesogens represent, in fact, the main goal of many different studies on such liquid crystal materials [9–11].

In order to investigate the possible correlations between the solid state and the liquid crystalline phase, we have reported several single crystal X-ray structure determinations of chloro-bridged orthopalladated compounds [12–14]. Continuing this area of investigation, in this paper we report the synthesis, the molecular structure determined by X-ray and the mesomorphic properties of the complex $[(\mathbf{Azo\text{-}6})Pd(\mu\text{-}Cl)]_2$, **1**, [**H(Azo-6)** = 4,4′-hexyloxyazobenzene].

The mesophases of complex **1**, detected through polarizing microscopic observations and differential scanning calorimetry (DSC), were also investigated by X-ray diffraction measurements (XRD) performed on the powder sample as a function of the temperature.

2. Results and discussion

Compound **1** is a cyclometallated chloro-bridged dimer obtained by palladation of the mesogen 4,4′-hexyloxyazobenzene, [**H(Azo-6)**: C→(108°C)N→(116°C)I].

The thermal behaviour of complex **1** was investigated by optical microscopy and differential scanning calorimetry (DSC).

When the sample is heated from room temperature, it melts to a nematic mesophase at 210°C displaying a typical schlieren texture. On further heating, the nematic phase gradually disappears, and the sample becomes increasingly dark, making further optical observations difficult. Decomposition eventually takes place at about

*Author for correspondence.

0267–8292/96 $12·00

235°C. The melting peak corresponds to an enthalpy (ΔH) of 40·7 J g^{-1} and an entropy (ΔS) of 83·7 J(g K)$^{-1}$. In addition, a further phase transition is observed by DSC corresponding to an endothermic peak centred at 220°C, with ΔH and ΔS of 0·72 J g^{-1} and 1·46 J(g K)$^{-1}$, respectively, and the decomposition peak is detected at 235°C.

In order more fully to characterize the behaviour of complex **1** as a function of temperature, X-ray single crystal analysis and variable temperature X-ray powder diffraction studies have been performed.

2.1. *Molecular structure*

Suitable crystals of the complex **1** were obtained by slow evaporation of a chloroform solution. The molecular structure of **1**, determined by single crystal X-ray analysis, is shown in figure 1. Compound **1**, (the *bis*(μ-chloro)cyclopalladated complex), crystallizes as discrete molecules in the monoclinic space group $P2_1/c$.

The dimer consists of two Pd(II) centres in a distorted square planar coordination, bridged by chlorine ligands. The coordination of each metal is completed by cyclometallation of two azobenzene ligands in a *trans*-geometry with respect to the Pd–Pd vector. As reported in table 1, the bond distances and angles are found to be in good agreement with those observed for similar compounds.

The Pd_2Cl_2 fragment in the molecule exhibits a slight folding, the dihedral angle between the two $PdCl_2$ planes being 14·5(1)°. Consequently, the Pd–Pd non-bonded distance of 3·528(1) Å, which is similar to that reported for dimeric chloro-bridged cyclopalladated azobenzenes [12], is longer than the corresponding value found in the analogous bent derivative of *N*-(4-methoxybenzylidene)-4′-butylaniline (3·326(2) Å for a dihedral angle of 38·7(3)°) [15]. The two five-membered chelate rings in complex **1** are essentially planar and form dihedral angles of 0·8(2) and 2·2(1)° with respect to the mean Pd_2Cl_2 plane.

The two metallated azobenzene ligands adopt the typical *trans*-configuration as the torsion angles about the central bond –N=N– are 177·1(8) and 177·4(8)°, respectively. The planarity of the entire azobenzene fragment observed for unmetallated diphenylazobenzenes [16] is partially retained after the orthometallation. Thus, the mean torsion angles –N–N–C(ar)–C(ar)– (of 4·5(1) and 1·0(2)°) for the orthometallated phenyl rings in complex **1** are indicative of a coplanarity with the respective metallacycles. On the other hand, the two rotationally free phenyl rings are tilted by 35·3(8) and 38·7(7)°, probably due to steric repulsion involving the bridging chlorine atoms. However, the deviations from planarity are less pronounced than for examples in which non-hydrogen atoms are in the *ortho*-positions [13, 14, 17].

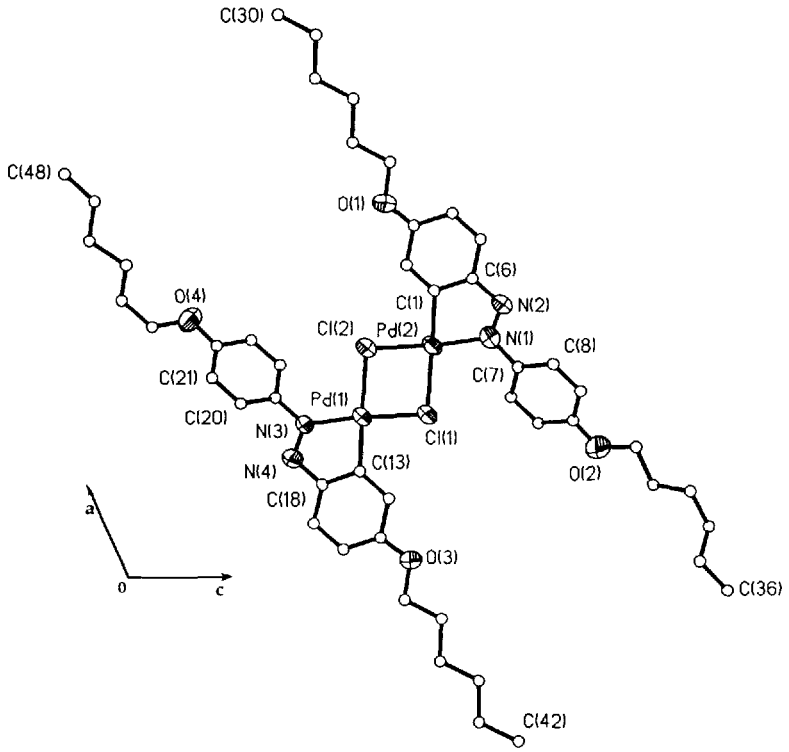

Figure 1. View of Complex **1** with the atomic numbering scheme along the *b* axis.

Table 1. Selected bond lengths (Å) and angles (°) in complex **1**.

Pd(1)–Cl(1)	2·332 (3)	Pd(2)–Cl(1)	2·469 (2)
Pd(1)–Cl(2)	2·463 (2)	Pd(2)–Cl(2)	2·328 (3)
Pd(1)–N(1)	2·055 (8)	Pd(2)–N(3)	2·040 (7)
Pd(1)–C(1)	1·968 (9)	Pd(2)–C(13)	1·949 (8)
N(1)–N(2)	1·265 (9)	N(3)–N(4)	1·280 (9)
N(1)–C(7)	1·438 (15)	N(2)–C(6)	1·372 (16)
N(3)–C(19)	1·417 (14)	N(4)–C(18)	1·374 (15)
C(1)–C(6)	1·410 (14)	C(13)–C(18)	1·419 (13)
Cl(1)–Pd(1)–Cl(2)	84·5 (1)	Cl(1)–Pd(2)–Cl(2)	84·4 (1)
Cl(1)–Pd(1)–N(1)	172·3 (2)	Cl(1)–Pd(2)–N(3)	102·1 (2)
Cl(2)–Pd(1)–N(1)	102·1 (2)	Cl(2)–Pd(2)–N(3)	172·7 (2)
Cl(1)–Pd(1)–C(1)	93·9 (3)	Cl(1)–Pd(2)–C(13)	175·8 (3)
Cl(2)–Pd(1)–C(1)	175·3 (3)	Cl(2)–Pd(2)–C(13)	93·7 (3)
N(1)–Pd(1)–C(1)	79·2 (4)	N(3)–Pd(2)–C(13)	79·5 (4)

The four *n*-hexyloxy chains adopt different conformations. Whilst the two chains from O(1) to C(30) and from O(3) to C(42) (figure 1) are in an antiperiplanar conformation with all torsion angles between 173 and 179°, the other two chains present a torsion angle of 100° about C(33)–C(34) and of 118° about C(43)–C(44), respectively.

As shown in figure 1, the whole molecule is elongated along the crystallographic *a* axis and inclined at 13·4° to it. Consequently, the long axis of the molecule forms an angle of 128·4° with respect to the *c* axis, while it is practically perpendicular to the *b* axis. The calculated length of the molecule (distance between terminal carbon atoms) is 25·6 Å.

2.2. *Molecular packing*

The molecular arrangement of the title complex in its crystalline phase is shown in the packing diagrams, figure 2.

In the unit cell, the molecules related by a centre of inversion present the shortest Pd–Pd non-bonded intermolecular interaction; the Pd(2)–Pd(2a) separation of 3·668(1) Å is only 0·14 Å longer than the Pd–Pd intramolecular separation (figure 2(*a*)). This feature suggests that the centrosymmetrically related molecules tend to pair in the crystal structure. These molecules are superimposed along the shortest axis of the unit cell (*b* axis) and are shifted by a transverse slip of 3·7 Å. The repetition of the unit cell along the *b* axis gives rise to a distribution of the metal atoms about the column axis in an almost zig-zag fashion (figure 2(*b*)).

Complex **1** crystallizes in the monoclinic space group $P2_1/c$, as mentioned previously. This space group is one of those which allows a closest packed arrangement of molecules [18]. The calculated value of the packing coefficient, $k=0{\cdot}74$, shows that the molecules of complex **1** are indeed close packed [19]. Figure 2(*c*) shows that each dimeric unit is surrounded by six pairs of molecules. This is consistent with the coordination 6 in a layer, provided in cases of closest packing [19].

2.3. *Variable temperature X-ray diffraction studies*

The XRD patterns of complex **1**, obtained at different temperatures, between room temperature (RT) and the isotropization point, in the first heating cycle, are shown in figure 3. The RT spectrum (A in figure 3) is typical of a crystalline solid phase. With increasing temperature, the structure of the RT crystalline phase undergoes no appreciable modifications up to $T=210$°C where a transition to a nematic mesophase is observed (B in figure 3). The same spectrum of a nematic mesophase is also observed at $T=215$°C. The diffuse peak in the small-angle region, which arises from correlations in the molecular arrangement along the director, corresponds to an average molecular length, *d*, of 23·8 Å. This value, less than the length of the molecule in the fully extended conformation, $L=25{\cdot}6$ Å (experimental value from the molecular structure of complex **1**, see §2.1), is due to the tilt effect associated with the orientational disorder [20, 21].

Further increase of the temperature above 220°C results in the formation of a mesophase which is more ordered than the nematic. In fact, as seen in C in figure 3, the diffraction pattern recorded at $T=230$°C has three sharp reflections (whose Bragg spacings are in the ratio 1 : 2 : 3) in the low-angle region of the spectrum and two very weak signals in the wide-angle region, centred at $2\theta=25{\cdot}4°$ and $2\theta=28{\cdot}4°$. A careful consideration of the partially diffuse signal at $2\theta=25{\cdot}4°$ suggests it is comprised of two or more strongly overlapping Bragg components.

The above pattern is characteristic of a layered structure typical of a smectic mesophase, whose layer thickness, *d*, is 25·3 Å as deduced from the Bragg spacings of the low-angle reflections. Since the value of the layer thickness is very close to the length *L* of the molecule

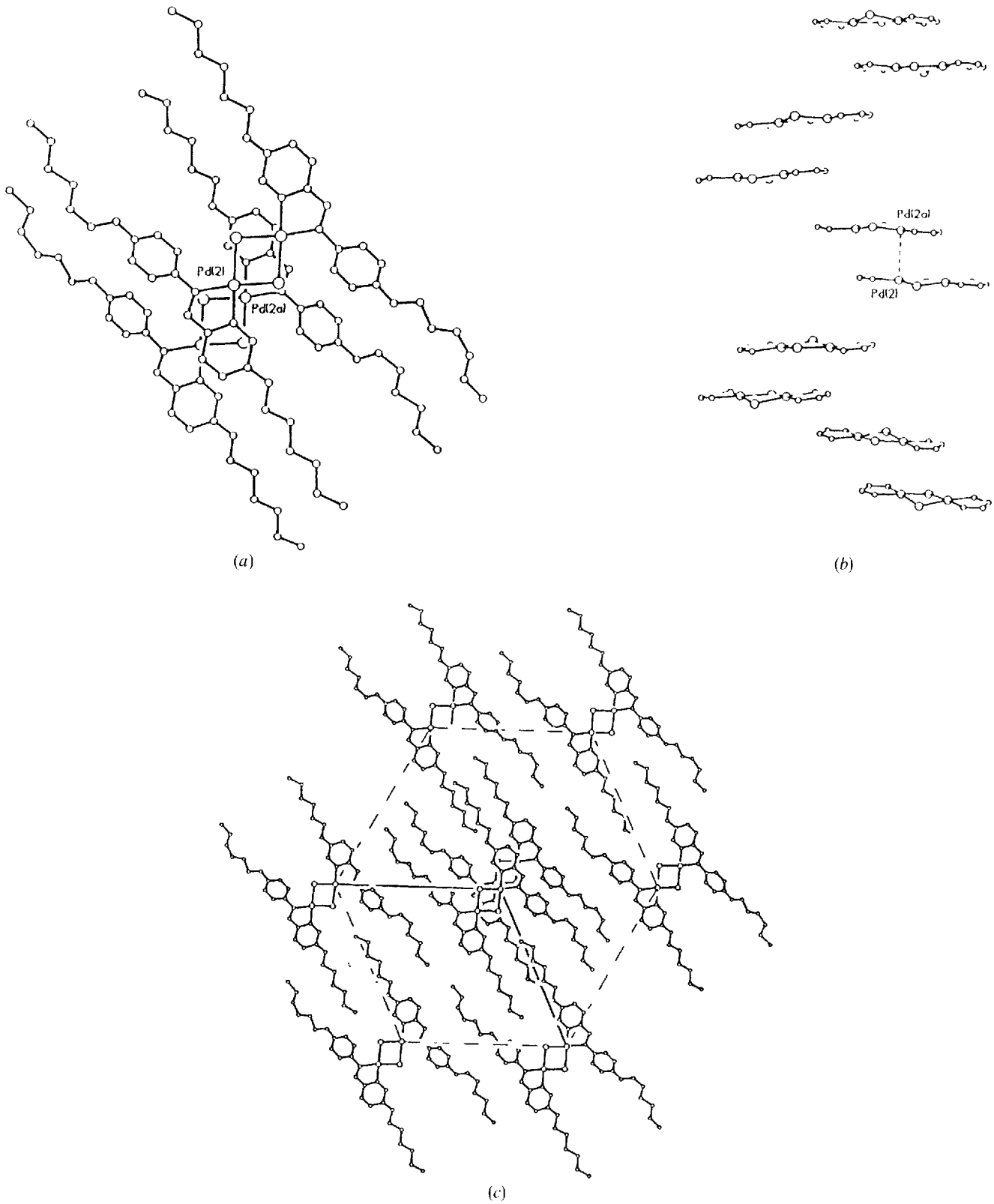

Figure 2. Crystal structure of Complex **1**. (*a*) Pair of molecules related by a centre of inversion viewed along the *b* axis; (*b*) Crystal packing projection down the *a* axis and (*c*) the *b* axis.

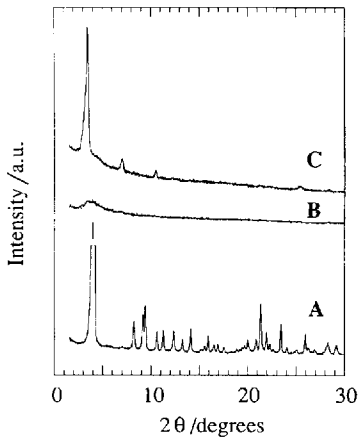

Figure 3. X-ray diffraction patterns of complex **1** obtained at different temperatures, between room temperature and the isotropization point in the first heating cycle: (A) $T=27°C$; (B) $T=214°C$; (C) $T=230°C$.

in the fully extended conformation, $L=25{\cdot}6$ Å, (experimental value from the molecular structure of complex **1**, see §2.1), we conclude that the mesophase is of the orthogonal type, i.e. the average direction of the molecular long axis is perpendicular to the layer planes. In addition, the complete absence in the wide-angle region of the broad diffuse signal, typical of disordered smectic structures and associated with short range liquid-like positional order within the layer, excludes the possibility of this mesophase being smectic A or C. However, the features of the wide-angle region of the spectrum centred about 25·4 and 28·4 degrees point to the existence of some long range positional order within the layers. These two reflections are not compatible with the hexagonal packing of a smectic B phase. On the other hand, the extreme weakness of the wide-angle signal does not allow the resolution of the structured peak at 25·4 degrees into its Bragg components. The conclusion from the experimental data is that the molecules are arranged within the layers in a quasi-hexagonal close-packed array, characteristic of the crystal E phase, but the resolution of the spectra in the wide-angle region prevents the determination of the unit cell parameters.

On further increasing the temperature, the E phase persists up to ~240°C where the palladium complex eventually decomposes.

2.4. *Concluding remarks*

A schematic representation of the crystal structure of complex **1** viewed along the *b* axis is shown in figure 4. The crystal has a smectic-like layer structure with the layer planes parallel to the *bc* plane. The molecular long axis is significantly tilted (51·6°, see §2.2) in the smectic-like layer and the layer spacing is 20·1 Å. Following the changes of the *d* parameter on going from the crystalline

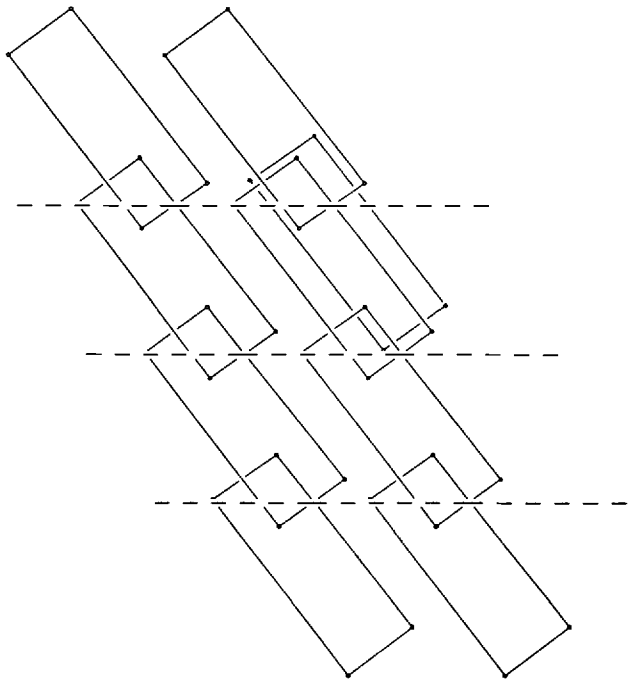

Figure 4. Schematic representation of the smectic-like layer structure of the crystal phase of Complex **1** viewed along the *b* axis. The smectic-like planes are indicated by dashed lines.

phase to the E phase, we observe a gradual increase, 20·1, 23·8 and 25·3 Å. The *d* value tends towards the length of the extended molecule, $L=25{\cdot}6$ Å, implying that the molecules change their tilt angle from 51·6 to 0° through the Cr to E transitions.

In a previous paper we reported on X-ray investigations performed either on powder samples or on monodomains of a homologous series of chloro-bridged cyclopalladated 4-C_nH_{2n+1}, 4′-C_mH_{2m+1} O-azobenzenes, having $n \neq m$ [22]. With reference to the molecular lengths estimated for the mesophases, values significantly lower than those theoretically calculated were obtained. On the basis of such evidence, a molecular array wherein the two alkyl chains are fused or bent toward each other was proposed. In compound **1**, the two alkoxy groups bear the same number of carbon atoms, and the calculated and the experimental values of the molecular length (25·1 and 25·6 Å, respectively) are similar. Consequently, in the present case the molecules in the nematic or in the E phase, could probably be better described by considering them with partially fused alkoxy chains only.

With reference to the mesomorphic behaviour, both the DSC and the XRD data show that an enantiotropic phase transition does take place at 220°C. Below this temperature the mesophase is nematic (optical and X-ray evidence) and turns into the E phase on increasing the temperature (XRD spectra, C in Figure 3).

Although re-entrant nematic phases can occur, it should be pointed out that they tend to appear below disordered smectic phases such as smectic A [23]. Alternatively, the N⇌E transition detected for **1** could be ascribed to a different phenomenon. In particular, we comment on the observed situation in the crystalline solid where the molecules of complex **1** are actually organized in pairs (figure 2(*a*)). In the pair, the interactions between the molecules are such that the non-bonding Pd–Pd intermolecular separation is 3·67 Å. Given that DSC measurements show an endothermic peak ($\Delta H = 0{\cdot}72\,J\,g^{-1}$) at 220°C, we suggest that during the heating cycle the molecular pairs dissociate giving rise to a uniform array of single molecules. Approached thus, the reversible N⇌E transition observed at 220°C could actually be coupled to a (molecules in a pair) ⇌(single molecule) transition like that previously observed for the mesomorphic Pd-(octyloxydithiobenzoate)$_2$ [24].

The nematic phase however is not in thermodynamic equilibrium and when subjected to an annealing process transforms into the E phase. This was experimentally verified by performing XRD measurements at a constant temperature using different acquisition times. The resulting spectra recorded at constant temperature, $T =$ 215°C, after times varying between 20 and 90 min, are shown in figure 5. The inset in the same figure shows the time evolution of the integrated intensity of the Bragg first order reflection, which gives a measure of the kinetics of the transformation. Further experimental evidence of the occurrence of the E phase with increasing time was found microscopically: on heating the sample and simply holding the temperature at 218°C for 10 min, we were able to see a new pseudo-solid phase growing

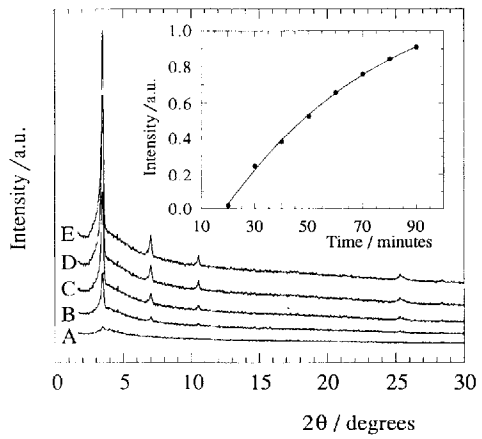

Figure 5. X-ray diffraction patterns of complex **1** recorded at $T = 215$°C after different acquisition times: (A) 20 min, (B) 40 min, (C) 60 min, (D) 80 min, (E) 90 min. The inset shows the time evolution of the integrated intensity of the first order Bragg reflection.

and forming from the nematic phase. This smectic-like phase, which exhibits a mosaic texture [25], is ordered and shows an XRD pattern (figure 5) which compares well to that of the mesophase (E phase) detected above 220°C (C in figure 3).

On the basis of these results alone we are not able to conclude with certainty whether the two phases displayed by **1** above and below 220°C are truly the same. However, since at 220°C we suggest a N(pair)⇌E(single) transition, what happens at a constant temperature between 213 and 220°C could be tentatively ascribed to a N(pair) → E(pair) trasformation where the E(pair) phase, at present, is indistinguishable from the E(single) phase.

The main difference between the two smectic-like phases, characterized by the single or paired nature of the molecules which build up the structure, lies in the short range positional order. This difference should be reflected in the features of the wide-angle region of the X-ray diffraction patterns. However, in the present case, the wide-angle signal is extremely weak and the resolution is not sufficient to solve the fine details of the spectra, which prevents determination of any significant differences in the short range order of the structures. Higher resolution experiments on oriented monodomains could provide more information.

In conclusion, for the palladium mesogen **1**, the transition from the low-temperature highly ordered crystalline phase to the high-temperature less ordered E phase takes place via a disordered nematic mesophase. This process is probably coupled with structural modifications of the mesogenic species, i.e. pairs of molecules (nematic phase) or single molecules (the E phase). Moreover, in the temperature range where the nematic mesophase is observed, the sample is not in thermodynamic equilibrium, i.e. the nematic mesophase is metastable and, at constant temperature, transforms into a layered phase with time.

The thermal behaviour of complex **1** is therefore very unusual. In order to check the actual rôle which intermolecular forces play in the mesomorphism of the dinuclear cyclopalladated species, further investigation is required. Studies dealing with complexes having a different halo-bridge, as well as complexes having greater thermal stability than **1**, are currently under way.

3. Experimental section

The synthesis of complex **1** was carried out as previously reported [26]. The textures of the mesophases were observed by means of a Zeiss Axioscope polarizing microscope equipped with a controlled hot stage plate, and the thermal behaviour was detected by means of a Perkin-Elmer DSC 7 with a heating/cooling rate of 10°C min^{-1}.

3.1. *X-Ray structure determination*

The crystallographic data for complex **1** are reported in table 2. The X-ray data collection was performed on a Siemens R3m/V four circle diffractometer, using graphite-monochromated MoK_α radiation ($\lambda = 0{\cdot}71069$ Å) and a 2θ scan. Lorentz and polarization corrections were applied to the intensity data, while absorption and extinction corrections were ignored. The structure was solved by using standard Patterson methods and completed by Fourier recycling.

The refinement was performed using a full-matrix least-squares procedure minimizing the function $\Sigma w(|F_o| - |F_c|)^2$. The weighting scheme used in the last refinement cycle was $w = 1{\cdot}00/\sigma^2(F_o) + 0{\cdot}0004(F_o)^2$. Only the Pd, Cl, N and oxygen atoms were refined anisotropically and the hydrogen atoms were positioned in calculated positions with common thermal parameters ($U = 0{\cdot}08$ Å^2). Some disorder was found in two of the aliphatic chains (from C(30) to C(36) and from C(43) to C(48)). The refinement was carried out using geometric contraints for the carbon atoms (the distances C–C were assumed to be 1·53 Å). Of 8537 independent reflections ($R_{int} = 0{\cdot}85$ per cent) 4232 were unique with $I > 2\sigma(I)$. These data were used in the final refinement of 301 parameters to arrive at a residual of $R = 0{\cdot}060$ and $R_w = 0{\cdot}057$.

All calculations were performed with SHELXTL PLUS [27] and PARST [28] programs. Atomic scattering factors were as implemented in the SHELXTL PLUS program.

Table A1 listing positional parameters of non-hydrogen atoms, and tables A2–A5, listing bond distances, bond angles, thermal parameters, positional parameters of hydrogen atoms and observed and calculated structure factors are given in the Appendix.

3.2. *X-Ray diffraction*

X-ray diffraction measurements on the powder sample were performed with the INEL CPS 120 powder diffractometer equipped with a curved, position sensitive detector covering 120° in the scattering angle 2θ, with an angular resolution of 0·018°. Ge(1 1 1) monochromatized CuK_α radiation was used. The sample, ~1 mm thick, was placed between two thin Al sheets and fixed inside the circular hole of an Al sample holder. Heating was provided by a hot stage and the temperature of the sample was controlled within ±0·1°C by an automatic temperature regulator. An acquisition time of 20 min was used for each measurement at constant temperature. The integrated intensity of the small-angle Bragg reflection in the E phase was measured from the corresponding spectra after background subtraction, deconvolution for the instrumental resolution function and correction for the Lorentz and polarization factors [29].

Table 2. Crystallographic data for complex **1**.

formula	$C_{48}H_{66}Cl_2N_4O_4Pd_2$
molecular weight	1046·7
colour	orange
space group	$P2_1/c$
temperature/K	298
a/Å	18·942 (3)
b/Å	15·384 (2)
c/Å	18·271 (3)
β/°	114·90 (2)
V/Å^3	4829·3 (13)
Z	4
$\mu(MoK_\alpha)$/cm^{-1}	9·01
R	0·060
R_w	0·057
S	1·45

Financial supports from the Italian Ministero per l'Universita' e la Ricerca Scientifica e Tecnologica (MURST) e Consiglio Nazionale delle Ricerche (CNR) are gratefully acknowledged.

Appendix

Table A1. Atomic coordinates ($\times 10^4$) and equivalent isotropic displacement coefficients (Å$^2 \times 10^3$) for complex **1**.

	x	y	z	$U_{eq.}$
Pd(1)	1657 (1)	1240 (1)	1920 (1)	52 (1)
Pd(2)	198 (1)	1156 (1)	−74 (1)	50 (1)
Cl(1)	1625 (1)	1320 (2)	631 (1)	64 (1)
Cl(2)	230 (1)	1347 (2)	1203 (1)	65 (1)
N(1)	1828 (5)	1252 (5)	3108 (4)	57 (4)
N(2)	2519 (4)	1345 (6)	3636 (4)	67 (4)
N(3)	29 (4)	1051 (4)	−1249 (4)	44 (3)
N(4)	−674 (4)	1029 (5)	−1788 (4)	54 (4)
O(1)	4612 (4)	1222 (5)	2298 (4)	81 (3)
O(2)	−463 (4)	925 (5)	4213 (5)	88 (4)
O(3)	−2758 (3)	1131 (5)	−433 (4)	74 (3)
O(4)	2216 (4)	942 (5)	−2527 (5)	85 (4)
C(1)	2802 (5)	1254 (6)	2468 (5)	55 (2)
C(2)	3331 (5)	1216 (6)	2163 (6)	60 (3)
C(3)	4137 (6)	1264 (7)	2665 (6)	67 (3)
C(4)	4383 (7)	1368 (7)	3503 (7)	79 (3)
C(5)	3853 (6)	1382 (6)	3817 (6)	68 (3)
C(6)	3051 (6)	1327 (6)	3310 (6)	61 (3)
C(7)	1223 (5)	1218 (6)	3386 (5)	50 (2)
C(8)	1279 (5)	1711 (6)	4050 (5)	56 (3)
C(9)	732 (5)	1636 (6)	4338 (6)	57 (3)
C(10)	114 (6)	1075 (7)	3971 (6)	63 (3)
C(11)	41 (6)	596 (7)	3303 (6)	72 (3)
C(12)	599 (5)	676 (6)	3010 (6)	60 (3)
C(13)	−935 (5)	1113 (6)	−609 (5)	47 (2)
C(14)	−1486 (5)	1156 (6)	−305 (6)	52 (2)
C(15)	−2280 (6)	1096 (6)	−810 (6)	57 (3)
C(16)	−2539 (5)	993 (6)	−1644 (5)	53 (3)
C(17)	−2003 (5)	971 (6)	−1979 (6)	60 (3)
C(18)	−1206 (5)	1036 (6)	−1458 (5)	51 (2)

Table A1. (*continued*).

	x	*y*	*z*	$U_{eq.}$
C(19)	593 (5)	1083 (6)	−1568 (5)	48 (2)
C(20)	469 (5)	1563 (6)	−2244 (5)	55 (3)
C(21)	1006 (5)	1553 (6)	−2569 (6)	62 (3)
C(22)	1663 (6)	1035 (7)	−2232 (6)	68 (3)
C(23)	1794 (6)	569 (6)	−1540 (6)	63 (3)
C(24)	1277 (5)	613 (6)	−1207 (6)	57 (3)
C(25)	5435 (6)	1372 (7)	2765 (6)	69 (3)
C(26)	5834 (6)	1354 (7)	2216 (6)	74 (3)
C(27)	6699 (5)	1527 (7)	2620 (6)	68 (3)
C(28)	7093 (6)	1600 (8)	2075 (6)	82 (3)
C(29)	7959 (6)	1667 (8)	2470 (7)	84 (4)
C(30)	8335 (7)	1848 (8)	1924 (7)	107 (4)
C(31)	−445 (7)	1343 (8)	4903 (7)	94 (4)
C(32)	−1237 (8)	1044 (9)	4917 (9)	137 (6)
C(33)	−1340 (11)	1396 (13)	5531 (11)	204 (9)
C(34)	−2077 (9)	968 (11)	5634 (10)	171 (7)
C(35)	−2775 (8)	1306 (10)	5101 (9)	149 (6)
C(36)	−3404 (7)	1008 (8)	5403 (8)	127 (5)
C(37)	−3586 (6)	1094 (7)	−912 (6)	75 (3)
C(38)	−3959 (5)	1229 (7)	−362 (6)	74 (3)
C(39)	−4850 (5)	1174 (7)	−778 (6)	71 (3)
C(40)	−5228 (6)	1351 (7)	−212 (6)	78 (3)
C(41)	−6101 (6)	1275 (8)	−584 (7)	90 (4)
C(42)	−6453 (7)	1477 (8)	12 (8)	118 (5)
C(43)	2056 (7)	1290 (8)	−3288 (8)	102 (4)
C(44)	2612 (9)	1028 (11)	−3663 (10)	165 (7)
C(45)	3334 (8)	1296 (10)	−3216 (9)	142 (6)
C(46)	3847 (8)	1107 (10)	−3728 (9)	138 (6)
C(47)	4636 (8)	1335 (10)	−3249 (9)	153 (6)
C(48)	5209 (7)	1164 (8)	−3601 (8)	124 (5)

[a] Equivalent isotropic U are defined as one third of the trace of the orthogonalized U_{ij} tensor

Table A2. Bond lengths (Å) for complex **1**.

Pd(1)–Cl(1)	2·332 (3)	Pd(1)–Cl(2)	2·463 (2)
Pd(1)–N(1)	2·055 (8)	Pd(1)–C(1)	1·968 (9)
Pd(2)–Cl(1)	2·469 (2)	Pd(2)–Cl(2)	2·328 (3)
Pd(2)–N(3)	2·040 (7)	Pd(2)–C(13)	1·949 (8)
N(1)–N(2)	1·265 (9)	N(1)–C(7)	1·438 (15)
N(2)–C(6)	1·372 (16)	N(3)–N(4)	1·280 (9)
N(3)–C(19)	1·417 (14)	N(4)–C(18)	1·374 (15)
O(1)–C(3)	1·329 (16)	O(1)–C(25)	1·447 (11)
O(2)–C(10)	1·361 (16)	O(2)–C(31)	1·402 (16)
O(3)–C(15)	1·350 (15)	O(3)–C(37)	1·440 (11)
O(4)–C(22)	1·374 (16)	O(4)–C(43)	1·400 (16)
C(1)–C(2)	1·339 (17)	C(1)–C(6)	1·410 (14)
C(2)–C(3)	1·413 (13)	C(3)–C(4)	1·409 (16)
C(4)–C(5)	1·350 (19)	C(5)–C(6)	1·410 (12)
C(7)–C(8)	1·397 (14)	C(7)–C(12)	1·370 (12)
C(8)–C(9)	1·350 (17)	C(9)–C(10)	1·380 (13)
C(10)–C(11)	1·383 (16)	C(11)–C(12)	1·377 (18)
C(13)–C(14)	1·374 (16)	C(13)–C(18)	1·419 (13)
C(14)–C(15)	1·399 (12)	C(15)–C(16)	1·399 (14)
C(16)–C(17)	1·390 (17)	C(17)–C(18)	1·409 (12)
C(19)–C(20)	1·372 (14)	C(19)–C(24)	1·384 (12)
C(20)–C(21)	1·378 (17)	C(21)–C(22)	1·384 (14)
C(22)–C(23)	1·381 (15)	C(23)–C(24)	1·356 (17)
C(25)–C(26)	1·489 (18)	C(26)–C(27)	1·511 (13)
C(27)–C(28)	1·479 (18)	C(28)–C(29)	1·492 (14)
C(29)–C(30)	1·475 (21)	C(31)–C(32)	1·579 (22)
C(32)–C(33)	1·331 (29)	C(33)–C(34)	1·625 (29)
C(34)–C(35)	1·372 (19)	C(35)–C(36)	1·578 (25)
C(37)–C(38)	1·466 (18)	C(38)–C(39)	1·533 (13)
C(39)–C(40)	1·509 (18)	C(40)–C(41)	1·504 (14)
C(41)–C(42)	1·528 (21)	C(43)–C(44)	1·532 (26)
C(44)–C(45)	1·329 (19)	C(45)–C(46)	1·634 (26)
C(46)–C(47)	1·422 (18)	C(47)–C(48)	1·499 (25)

Table A3. Bond angles (°) for complex **1**.

Cl(1)–Pd(1)–Cl(2)	84·5 (1)	Cl(1)–Pd(1)–N(1)	172·3 (2)
Cl(2)–Pd(1)–N(1)	102·1 (2)	Cl(1)–Pd(1)–C(1)	93·9 (3)
Cl(2)–Pd(1)–C(1)	175·3 (3)	N(1)–Pd(1)–C(1)	79·2 (4)
Cl(1)–Pd(2)–Cl(2)	84·4 (1)	Cl(1)–Pd(2)–N(3)	102·1 (2)
Cl(2)–Pd(2)–N(3)	172·7 (2)	Cl(1)–Pd(2)–C(13)	175·8 (3)
Cl(2)–Pd(2)–C(13)	93·7 (3)	N(3)–Pd(2)–C(13)	79·5 (4)
Pd(1)–Cl(1)–Pd(2)	94·5 (1)	Pd(1)–Cl(2)–Pd(2)	94·8 (1)
Pd(1)–N(1)–N(2)	117·4 (8)	Pd(1)–N(1)–C(7)	125·3 (5)
N(2)–N(1)–C(7)	117·1 (8)	N(1)–N(2)–C(6)	112·2 (8)
Pd(2)–N(3)–N(4)	117·6 (7)	Pd(2)–N(3)–C(19)	128·2 (5)
N(4)–N(3)–C(19)	113·9 (7)	N(3)–N(4)–C(18)	112·3 (8)
C(3)–O(1)–C(25)	119·0 (8)	C(10)–O(2)–C(31)	119·7 (8)
C(15)–O(3)–C(37)	118·7 (7)	C(22)–O(4)–C(43)	117·9 (8)
Pd(1)–C(1)–C(2)	130·2 (7)	Pd(1)–C(1)–C(6)	110·3 (8)
C(2)–C(1)–C(6)	119·5 (8)	C(1)–C(2)–C(3)	121·4 (10)
O(1)–C(3)–C(2)	116·4 (9)	O(1)–C(3)–C(4)	124·6 (9)
C(2)–C(3)–C(4)	118·9 (12)	C(3)–C(4)–C(5)	120·0 (9)
C(4)–C(5)–C(6)	120·5 (10)	N(2)–C(6)–C(1)	120·4 (8)
N(2)–C(6)–C(5)	119·9 (9)	C(1)–C(6)–C(5)	119·7 (11)
N(1)–C(7)–C(8)	120·5 (8)	N(1)–C(7)–C(12)	119·5 (9)
C(8)–C(7)–C(12)	120·0 (10)	C(7)–C(8)–C(9)	120·1 (8)
C(8)–C(9)–C(10)	119·8 (10)	O(2)–C(10)–C(9)	125·6 (10)
O(2)–C(10)–C(11)	113·7 (9)	C(9)–C(10)–C(11)	120·8 (12)
C(10)–C(11)–C(12)	119·2 (9)	C(7)–C(12)–C(11)	120·1 (10)

Table A3. (*continued*).

Pd(2)–C(13)–C(14)	131·2 (6)	Pd(2)–C(13)–C(18)	111·3 (8)
C(14)–C(13)–C(18)	117·3 (7)	C(13)–C(14)–C(15)	121·3 (9)
O(3)–C(15)–C(14)	115·3 (9)	O(3)–C(15)–C(16)	123·9 (8)
C(14)–C(15)–C(16)	120·8 (11)	C(15)–C(16)–C(17)	119·8 (8)
C(16)–C(17)–C(18)	118·3 (9)	N(4)–C(18)–C(13)	119·0 (7)
N(4)–C(18)–C(17)	118·5 (9)	C(13)–C(18)–C(17)	122·4 (10)
N(3)–C(19)–C(20)	121·0 (8)	N(3)–C(19)–C(24)	120·1 (9)
C(20)–C(19)–C(24)	118·9 (10)	C(19)–C(20)–C(21)	120·3 (8)
C(20)–C(21)–C(22)	120·2 (10)	O(4)–C(22)–C(21)	125·2 (10)
O(4)–C(22)–C(23)	115·6 (9)	C(21)–C(22)–C(23)	119·2 (12)
C(22)–C(23)–C(24)	120·0 (9)	C(19)–C(24)–C(23)	121·3 (9)
O(1)–C(25)–C(26)	109·1 (8)	C(25)–C(26)–C(27)	114·9 (8)
C(26)–C(27)–C(28)	115·8 (8)	C(27)–C(28)–C(29)	116·4 (9)
C(28)–C(29)–C(30)	115·6 (9)	O(2)–C(31)–C(32)	102·5 (9)
C(31)–C(32)–C(33)	111·9 (13)	C(32)–C(33)–C(34)	111·8 (14)
C(33)–C(34)–C(35)	112·5 (15)	C(34)–C(35)–C(36)	106·6 (14)
O(3)–C(37)–C(38)	107·1 (8)	C(37)–C(38)–C(39)	113·6 (8)
C(38)–C(39)–C(40)	113·1 (8)	C(39)–C(40)–C(41)	115·2 (9)
C(40)–C(41)–C(42)	112·9 (9)	O(4)–C(43)–C(44)	116·1 (10)
C(43)–C(44)–C(45)	111·5 (15)	C(44)–C(45)–C(46)	107·4 (14)
C(45)–C(46)–C(47)	109·2 (13)	C(46)–C(47)–C(48)	117·2 (13)

Table A4. Anisotropic displacement coefficients ($Å^2 \times 10^3$) for complex **1**.

	U_{11}	U_{22}	U_{33}	U_{12}	U_{13}	U_{23}
Pd(1)	46 (1)	62 (1)	37 (1)	−1 (1)	6 (1)	−1 (1)
Pd(2)	45 (1)	62 (1)	36 (1)	−1 (1)	8 (1)	−1 (1)
Cl(1)	48 (1)	90 (2)	42 (1)	−3 (1)	9 (1)	3 (1)
Cl(2)	49 (1)	99 (2)	38 (1)	4 (2)	9 (1)	−5 (1)
N(1)	61 (5)	57 (5)	48 (5)	−1 (5)	18 (4)	−1 (5)
N(2)	48 (5)	101 (7)	43 (5)	−4 (5)	9 (4)	1 (5)
N(3)	41 (4)	53 (5)	35 (4)	−3 (4)	13 (4)	−5 (4)
N(4)	44 (5)	63 (6)	49 (5)	−6 (4)	13 (4)	−6 (4)
O(1)	43 (4)	122 (6)	68 (5)	−5 (5)	14 (3)	1 (5)
O(2)	67 (5)	115 (7)	85 (6)	−17 (5)	34 (4)	−13 (5)
O(3)	40 (4)	117 (6)	62 (4)	−4 (4)	19 (3)	−4 (5)
O(4)	77 (5)	105 (6)	89 (6)	7 (4)	50 (5)	10 (5)

The anisotropic displacement factor exponent takes the form:
$-2\pi^2(h^2a^{*2}U_{11} + \ldots + 2hka^*b^*U_{12})$

Table A5. H-Atom coordinates ($\times 10^4$) and isotropic displacement coefficients ($Å^2 \times 10^3$) for complex **1**.

	x	y	z	$U_{eq.}$
H(2)	3160	1155	1591	80
H(4)	4926	1430	3849	80
H(5)	4023	1430	4390	80
H(8)	1707	2104	4303	80
H(9)	772	1973	4797	80
H(11)	−394	212	3046	80
H(12)	552	353	2543	80
H(14)	−1322	1229	265	80
H(16)	−3085	938	−1983	80
H(17)	−2171	914	−2551	80
H(20)	6	1908	−2491	80
H(21)	925	1906	−3031	80
H(23)	2251	215	−1296	80

Table A5. (*continued*).

H(24)	1387	312	−710	80
H(25a)	5512	1929	3025	80
H(25b)	5646	925	3166	80
H(26a)	5755	790	1969	80
H(26b)	5598	1787	1807	80
H(27a)	6939	1059	2990	80
H(27b)	6778	2062	2914	80
H(28a)	6960	1095	1735	80
H(28b)	6896	2110	1750	80
H(29a)	8161	1126	2738	80
H(29b)	8096	2127	2860	80
H(30a)	8888	1879	2231	80
H(30b)	8148	2392	1654	80
H(30c)	8213	1391	1532	80
H(31a)	−7	1154	5380	80
H(31b)	−427	1963	4855	80

Table A5. (*continued*).

H(32a)	−1235	423	4965	80
H(32b)	−1659	1219	4422	80
H(33a)	−879	1303	6019	80
H(33b)	−1428	2009	5437	80
H(34a)	−2021	1073	6174	80
H(34b)	−2079	353	5544	80
H(35a)	−2747	1929	5098	80
H(35b)	−2905	1088	4568	80
H(36a)	−3905	1232	5046	80
H(36b)	−3267	1226	5938	80
H(36c)	−3425	385	5408	80
H(37a)	−3742	1541	−1315	80
H(37b)	−3729	536	−1168	80
H(38a)	−3772	794	52	80
H(38b)	−3816	1795	−122	80
H(39a)	−4994	601	−998	80
H(39b)	−5037	1593	−1206	80
H(40a)	−5094	1932	−8	80
H(40b)	−5022	945	226	80
H(41a)	−6312	1675	−1027	80
H(41b)	−6241	693	−779	80
H(42a)	−7009	1419	−255	80
H(42b)	−6321	2061	208	80
H(42c)	−6250	1078	456	80
H(43a)	1541	1109	−3650	80
H(43b)	2070	1912	−3241	80
H(44a)	2434	1281	−4191	80
H(44b)	2612	406	−3706	80
H(45a)	3334	1907	−3109	80
H(45b)	3548	983	−2715	80
H(46a)	3649	1448	−4213	80
H(46b)	3815	501	−3865	80
H(47a)	4651	1946	−3138	80
H(47b)	4805	1015	−2753	80
H(48a)	5719	1343	−3224	80
H(48b)	5061	1485	−4094	80
H(48c)	5216	554	−3709	80

References

[1] GHEDINI, M., ARMENTANO, S., and NEVE, F., 1987, *Inorg. Chim. Acta*, **134,** 23.

[2] OSHINO, N., HASEGAWA, H., and MATSUMAGA, Y., 1991, *Liq. Cryst.*, **9,** 267.

[3] ROS, M. B., Ruiz, N., SERRANO, J. L., and ESPINET, P., 1991, *Liq. Cryst.*, **9,** 77.

[4] PRAEFCKE, K., SINGER, D., and GÜNDOGAN, B., 1992, *Mol. Cryst. liq. Cryst.*, **223,** 181.

[5] BRUCE, D. W., and O'HARE, D., (eds) 1992, *Inorganic Materials* (Chichester, UK: Wiley).

[6] GIROUD-GODQUIN, A. M., and MAITLIS, P. M., 1991, *Angew. Chem., Int. Ed. Engl.*, **30,** 375.

[7] ESPINET, P., ESTERUELAS, M. A., ORO, L. A., SERRANO, J. L., SOLA, E., 1992, *Coord. Chem. Rew.*, **117,** 215.

[8] HUDSON, S. A., and MAITLIS, P. M., 1993, *Chem. Rev.*, **93,** 861.

[9] USHA, K., VIJAYAN, K., CHANDRASEKHAR, S., 1993, *Liq. Cryst.*, **15,** 575.

[10] USHA, K., SADASHIVA, B. K., VIJAYAN, K., 1994, *Mol. Cryst. liq. Cryst.*, **241,** 91.

[11] ATENCIO, R., BARBERÀ, J., CATIVIELA, C., LAHOZ, F. J., SERRANO, J. L., and ZURBANO, M. M., 1994, *J. Am. chem. Soc.*, **116,** 11558.

[12] ARMENTANO, S., CRISPINI, A., DE MUNNO, G., GHEDINI, M., and NEVE, F., 1991, *Acta Crystallogr.*, **C47,** 2545.

[13] ARMENTANO, S., CRISPINI, A., DE MUNNO, G., GHEDINI, M., and NEVE, F., 1991, *Acta Crystallogr.*, **C47,** 966.

[14] CRISPINI, A., DE MUNNO, G., GHEDINI, M., and NEVE, F., 1992, *J. Organomet. Chem.*, **427,** 409.

[15] GHEDINI, M., ARMENTANO, S., DE MUNNO, G., CRISPINI, A. and NEVE, F., 1990, *Liq. Cryst.*, **8,** 739.

[16] KLEBE, G., 1994, *J. Mol. Struct. (Teochem)*, **308,** 53.

[17] CRISPINI, A., GHEDINI, M., and NEVE, F., 1993, *J. Organomet. Chem.*, **448,** 241.

[18] KITAIROGODSKII, A. I., 1973, *Molecular Crystals and Molecules* (New York: Academic Press), p. 33.

[19] KITAIROGODSKII, A. I., 1955, *Organic Chemical Crystallography* (New York: Consultans Bureau Enterprises Inc.), p. 13.

[20] LEADBETTER, A. J., RICHARDSON, R. H., and COLLING, C. N., 1975, *J. Phys. (Paris)*, **36,** C1.

[21] DE VRIES, A., 1973, *Liq. Cryst.*, **20,** 119.

[22] LEVELUT, A. M., VEBER, M., FRANCESCANGELI, O., MELONE, S., GHEDINI, M., NEVE, F., NICOLETTA, F. P., and BARTOLINO, R., 1995, *Liq. Cryst.* **19,** 241.

[23] DE GENNES, P. G., and PROST, J., 1995, *The Physics of Liquid Crystals* (Oxford: Clarendon Press), p. 568.

[24] GUILLON, D., BRUCE, D. W., MALDIVI, P., IBN-ELHAJ, M., and DHILLON, R., 1994, *Chem. Mater.*, **6,** 182.

[25] GRAY, G. W., and GOODBY, J. W., 1984, *Smectic Liquid Crystals – Textures and Structures* (Glasgow: Heiden and Son Ed.), p. 82.

[26] GHEDINI, M., PUCCI, D., CESAROTTI, E., ANTOGNIAZZA, P., FRANCESCANGELI, O., and BARTOLINO, R., 1993, *Chem. Mater.*, **5,** 883.

[27] SHELXTL PLUS, 1990, Version 4.21, Siemens Analytical X-ray Instruments Inc., Madison, WI.

[28] NARDELLI, M., 1983, *Comp. Chem.*, **7,** 95.

[29] CULLITY, B. D., 1978, *Elements of X-ray Diffraction* (Reading, Massachusetts: Addison-Wesley), p. 130.